When Active Learning Meets Graph Similarity: Evidential Variance for Graph Selection

Anonymous authors
Paper under double-blind review

Abstract

Graph Similarity Learning (GSL) is pivotal in graph data mining, yet training effective models necessitates substantial labeled pairs, which incur prohibitive annotation costs. To address this, we introduce Active Learning (AL) into the GSL paradigm. However, directly transferring existing AL strategies is non-trivial due to two unique impediments: (1) the *continuous regression nature* of similarity prediction complicates standard uncertainty quantification, and (2) the *paired-input structure* requires evaluating a graph's informational value across its pairings rather than in isolation. To bridge this gap, we propose **EVGS** (Evidential Variance for Graph Selection), a novel AL framework tailored for GSL. EVGS leverages evidential deep learning to impose a prior over predictions, enabling disentangled uncertainty estimation. Crucially, we identify a "gradient shrinkage" pathology inherent to the data-scarce regime characteristic of AL cycles. We introduce a novel MSE-anchored regularizer to mitigate this issue, ensuring discriminative uncertainty estimation even with limited labels. Furthermore, to address the paired-input challenge, we propose a graph-centric selection criterion: *uncertainty variance*. This metric captures a graph's holistic informational value by measuring fluctuations in its epistemic uncertainty across diverse interactions. Extensive experiments on three benchmarks with two GSL backbones demonstrate that EVGS consistently outperforms established AL baselines.

1 Introduction

Graph-structured data is ubiquitous in modeling complex relationships across diverse domains, ranging from social networks to chemical molecules (Ju et al., 2025). In these contexts, measuring graph similarity serves as a fundamental task, underpinning critical applications such as graph retrieval, malware detection, and brain network analysis (Ma et al., 2021). While traditional algorithms like Graph Edit Distance (GED) (Gao et al., 2010) provide exact metrics, they are known to be NP-complete (Bunke & Shearer, 1998), rendering them computationally prohibitive for large-scale real-world datasets.

To circumvent this computational bottleneck, recent research has pivoted towards **Graph Similarity Learning (GSL)**, which leverages Graph Neural Networks (GNNs) (Wu et al., 2020) to efficiently approximate similarity metrics (Li et al., 2019; Wang et al., 2021; Ranjan et al., 2022; Tan et al., 2023; Lan et al., 2024; Zheng et al., 2025; Zou et al., 2025). By training on annotated graph pairs, GSL models, including both embedding-based (Bai et al., 2019; Zhang et al., 2021d) and interaction-based architectures (Ling et al., 2019; Xu et al., 2021), enable rapid similarity inference on unseen graph pairs.

Despite their promising performance, a critical limitation persists: these data-driven models are notoriously data-hungry (Li et al., 2018). Obtaining the necessary ground-truth labels (e.g., exact GED values) requires running expensive algorithms on massive datasets, creating a paradoxical situation where training an efficient model incurs a prohibitive initial cost (Cai et al., 2017). For example, training a standard GSL model such as SimGNN (Bai et al., 2019) often demands millions of labeled pairs, imposing a severe annotation burden (Sorokin & Forsyth, 2008). Consequently, **Active Learning (AL)** (Settles, 2009) emerges as a vital solution, offering a principled framework to strategically select only the most informative samples for annotation, thereby maximizing performance under limited budgets.

However, adapting AL strategies from general machine learning (Settles, 2009; Ren et al., 2021) to the GSL domain is non-trivial due to a fundamental task mismatch. Existing graph AL methods predominantly focus on node classification (Gao et al., 2018; Zhang et al., 2021a; 2022; Sheng et al., 2025; Chen et al., 2026), typically selecting nodes based on prediction entropy. In contrast, GSL operates on graph pairs for similarity regression, presenting two inherent challenges that render off-the-shelf strategies ineffective:

- **Challenge 1: Uncertainty Quantification in Regression.** Unlike classification, where entropy naturally measures uncertainty over discrete classes, GSL outputs continuous similarity scores. Consequently, standard entropy-based metrics are inapplicable, necessitating alternative uncertainty measures that are compatible with the continuous output space of regression models.
- **Challenge 2: Structural Dependency in Paired Inputs.** GSL inputs are combinatorial pairs, yet the underlying information stems from individual graphs. Naive pair-level selection ignores this dependency: it treats each pair as an isolated instance, overlooking that a single graph participates in multiple relationships. Simply evaluating uncertainty at the pair level is myopic, failing to capture the graph's holistic information value for similarity-space learning. Therefore, effective selection must account for each graph's collective impact across its associated pairs.

To address these challenges, we propose **E**vidential **V**ariance for **G**raph **S**election (**EVGS**), a novel and general AL framework designed to identify the most informative graphs for GSL. EVGS tackles the aforementioned obstacles through two key innovations. First, to quantify regression uncertainty (Challenge 1), we adapt **evidential deep learning** (Sensoy et al., 2018; Amini et al., 2020) to place a higher-order prior over model predictions, enabling the joint estimation of aleatoric and epistemic uncertainty. Crucially, we identify a "gradient shrinkage" pathology in standard evidential learning within low-data regimes and introduce a novel **MSE-anchored regularizer**. This mechanism mitigates vanishing gradients, ensuring discriminative and reliable uncertainty estimation, a prerequisite for robust active selection. Second, to resolve the combinatorial dependency (Challenge 2), we introduce a new selection criterion: **uncertainty variance**. Instead of evaluating pairs in isolation, this metric computes the variance of a candidate graph's epistemic uncertainty across its interactions with other graphs. By prioritizing graphs that exhibit high variability in model confidence across different contexts, EVGS captures the holistic informational value of each graph. Importantly, EVGS is model-agnostic, seamlessly integrating with various GSL architectures to provide a versatile solution for data-efficient GSL. In summary, our main contributions are threefold:

- **Pioneering AL for GSL:** To the best of our knowledge, this is the first work to formalize AL specifically for GSL. We identify the unique challenges of applying AL to paired-input regression tasks, bridging the critical gap between data-efficient learning and graph matching.
- **Methodological Innovation:** We propose EVGS, a novel framework that synergizes evidential deep learning with a tailored MSE-anchored regularizer to mitigate gradient shrinkage, and introduces a structure-aware uncertainty variance metric to capture holistic informational value.
- **Empirical Validation:** Extensive experiments across three benchmarks and two GSL backbones show that EVGS consistently outperforms established AL baselines. Our results validate both the efficacy of our uncertainty estimation and the necessity of graph-centric selection strategies.

2 Related Work

2.1 Graph Similarity Learning (GSL)

Traditional approaches to graph similarity, exemplified by Graph Edit Distance (GED) (Gao et al., 2010) and Maximum Common Subgraph (MCS) (Bunke & Shearer, 1998), provide rigorous theoretical foundations but are computationally intractable. Specifically, the exact computation of these metrics is known to be NP-hard (Bunke & Shearer, 1998), rendering them impractical for large-scale real-world scenarios. To circumvent this scalability bottleneck, graph kernels (Yan et al., 2005; Yanardag & Vishwanathan, 2015; Nikolentzos et al., 2017) were introduced as an alternative; however, they often suffer from shallow expressiveness, limiting their generalization capabilities. Consequently, the field has witnessed a paradigm shift towards Graph Neural Networks (GNNs) (Wu et al., 2020; Ju et al., 2025). By learning expressive data-driven representations,

GNN-based GSL methods have achieved state-of-the-art performance across diverse applications (Li et al., 2019; Ma et al., 2019; Doan et al., 2021; Qin et al., 2021; Wang et al., 2021; Ranjan et al., 2022).

Early embedding-based approaches typically estimate similarity by comparing independently learned graph-level representations using metrics such as cosine or Hamming distance (Zhang et al., 2021d). To better capture substructural intricacies, SMPNN (Riba et al., 2018) and HGMN (Ling et al., 2019) introduced mechanisms to aggregate node-node similarity scores and model cross-graph interactions, respectively. Further enhancing granularity, SimGNN (Bai et al., 2019) incorporates a learnable neural tensor network with histogram features, while GraphSim (Bai et al., 2020) employs CNNs to process node similarity matrices as images. Subsequent research, including MGMN (Ling et al., 2021) and hierarchical approaches (Xu et al., 2020; 2021), explores multi-level matching and graph partitioning to facilitate effective cross-scale comparisons. Building upon these interaction-focused paradigms, NA-GSL (Tan et al., 2023) proposes a unified framework that leverages cross-graph co-attention and similarity-wise self-attention for precise structural alignment. Most recently, GraSP (Zheng et al., 2025) has advanced the boundaries of expressiveness and efficiency through multi-scale pooling and positional encodings. Parallelly, AMFF (Zou et al., 2025) introduces an adaptive feature fusion mechanism to dynamically adjust weights based on node-graph interactions.

Despite these architectural innovations, a critical bottleneck persists: existing models are predominantly data-hungry, requiring substantial annotated datasets to ensure generalization. This reliance incurs prohibitive annotation costs, especially given the complexity of labeling graph pairs. To address this challenge, we introduce a general Active Learning (AL) framework tailored explicitly for GSL.

2.2 Active Learning (AL)

Common AL. AL aims to maximize model performance under a limited budget by iteratively querying labels for the most valuable instances. Existing strategies generally fall into three categories: informativeness-based, representativeness-based, and hybrid approaches. Informativeness-based methods prioritize instances where the model is highly uncertain. Beyond classic techniques such as Uncertainty Sampling (Settles, 2009) and Query-by-Committee (QBC) (Seung et al., 1992), recent advances, such as Learning Loss (Yoo & Kweon, 2019), extend this paradigm to deep learning by training a module to predict the target loss of unlabeled samples. Representativeness-based approaches ensure the selected subset covers the underlying data distribution. While traditional methods rely on density (Xu et al., 2007) or clustering metrics (Nguyen & Smeulders, 2004), the influential Coreset (Sener & Savarese, 2018) algorithm adapts this to deep networks by formulating sample selection as a k-Center problem in the feature space. Hybrid strategies synergize these objectives to achieve a balance between uncertainty and diversity. For example, IR-AL (Yang et al., 2015) explicitly maximizes diversity within uncertainty sampling, while BADGE (Ash et al., 2020) selects samples with high gradient magnitudes (uncertainty indicator) that are simultaneously diverse in the gradient space.

AL on Graph. AL on graphs presents unique challenges, necessitating strategies that explicitly account for topological dependencies and relational complexities (Yang et al., 2025a;b). Initial efforts, such as AGE (Cai et al., 2017) and ANRMAB (Gao et al., 2018), adapted traditional criteria by incorporating node centrality and embedding density. Recognizing the importance of connectivity, subsequent methods like ALG (Zhang et al., 2021a) and Grain (Zhang et al., 2021c) focus on influence maximization, prioritizing nodes that effectively propagate information to their neighbors. Beyond structural heuristics, researchers have explored more sophisticated selection mechanisms. For example, SEAL (Li et al., 2020) and GALE (Guan et al., 2023) employ adversarial strategies to probe graph structures, while IGP (Zhang et al., 2022) introduces soft-labeling to mitigate annotation ambiguity. In parallel, several works address practical deployment constraints: RIM (Zhang et al., 2021b) tackles noisy oracles, and ALLIE (Cui et al., 2022) handles large-scale class imbalance. Most recently, FSV (Chen et al., 2026) offers a novel perspective by tracking feature dynamics, while DMA (Sheng et al., 2025) integrates dataset-specific characteristics with LLM capabilities.

Despite these advancements, a critical gap remains: existing graph AL methods mainly focus on *node classification*. In contrast, GSL operates on *graph pairs* for *similarity regression*. This fundamental divergence presents two inherent challenges: (1) the continuous nature of regression targets complicates uncertainty quantification, and (2) the combinatorial structure of paired inputs requires holistically evaluating a graph's value. To this end, we introduce EVGS, a general framework tailored for the paired-input regression task.

3 Preliminaries

3.1 Graph Similarity Learning

Definition 1 ***Graph Similarity Learning (GSL).*** *Let $\mathcal{G}$ be the space of all graphs. Given a pair of graphs $(G, G') \in \mathcal{G} \times \mathcal{G}$, GSL aims to learn a regression function $f : \mathcal{G} \times \mathcal{G} \to \mathbb{R}$ that predicts a similarity score $\hat{y}$ approximating the ground-truth metric y.*

Current GSL architectures typically employ Siamese GNNs. Given a pair (G, G'), a weight-sharing GNN encoder first extracts node representations $\mathbf{H}$ and $\mathbf{H}'$. A readout function then aggregates these into graph embeddings $\mathbf{g}$ and $\mathbf{g}'$. To capture the interaction between these two graphs, a fusion module ϕ constructs a graph-pair representation $\mathbf{z}$, which is subsequently mapped to the scalar similarity score by a regressor ψ:

$$\mathbf{z} = \phi(\mathbf{g}, \mathbf{g}', \mathbf{H}, \mathbf{H}'), \quad \hat{y} = \psi(\mathbf{z}). \tag{1}$$

While effective, training ϕ and ψ modules is data-hungry. Given the high cost of ground-truth annotation for GSL, we propose integrating AL to achieve high performance with minimal labeled data.

3.2 Pool-based Batch-mode Active Learning

In this work, we adopt the pool-based batch-mode active learning paradigm (Sugiyama & Nakajima, 2009; Cai et al., 2016) to maximize the sample efficiency of the GSL model f.

Problem Setup. The active learning process operates on the space of graph pairs, initialized with a small seed set $\mathbb{L}_0$ and a large unlabeled pool $\mathbb{U}_0 \subseteq \mathcal{G}_{\text{pool}} \times \mathcal{G}_{\text{pool}}$, where $\mathcal{G}_{\text{pool}}$ denotes the collection of available graphs. The learning procedure spans T rounds. In each round t, the GSL model f is trained on $\mathbb{L}_{t-1}$. Subsequently, a query strategy selects a batch Δ_t of informative pairs from $\mathbb{U}_{t-1}$ for annotation. The ground-truth similarity scores for Δ_t are queried from an Oracle (e.g., an exact GED solver), which is typically computationally intensive. The datasets are then updated as $\mathbb{L}_t \leftarrow \mathbb{L}_{t-1} \cup \Delta_t$ and $\mathbb{U}_t \leftarrow \mathbb{U}_{t-1} \setminus \Delta_t$.

Query Level: Pairs vs. Graphs. A fundamental challenge in active GSL arises from the combinatorial nature of the input space. While the GSL model and the Oracle operate on pairs, the underlying dataset is composed of individual graphs. This discrepancy necessitates a strategic choice regarding the selection level:

- Pair-level Selection: Treats the unlabeled pool as a flat set of independent pairs, directly selecting the most informative instances (G^i, G^j) to form the query pair batch Δ_t.
- Graph-centric Selection: Shifts the focus to individual graphs. Unlike direct pair sampling, this entails a *constructive process*: it first identifies a batch of critical graphs $\mathcal{G}_t \subseteq \mathcal{G}_{\text{pool}}$, and subsequently generates the query pair batch Δ_t by forming all pairwise constraints within $\mathcal{G}_t$. Finally, the candidate graph pool is updated: $\mathcal{G}_{\text{pool}} \leftarrow \mathcal{G}_{\text{pool}} \setminus \mathcal{G}_t$.

For both strategies, we define the annotation budget strictly in terms of the number of queried pairs per round. To maintain consistency across different selection levels, we align the number of selected graphs m with the pair budget $b = |\Delta_t|$. Specifically, under the graph-centric strategy where the query batch is constructed from all pairwise combinations within the selected graph set, the relationship is governed by $b = \binom{m}{2}$. This formulation allows us to derive the required graph batch size m for a given pair budget b. For example, selecting $m = 25$ graphs corresponds to an annotation cost of $b = 300$ pairs.

In this work, we advocate for the **graph-centric** strategy. We argue that standard pair-level selection is suboptimal because it treats similarity learning as isolated comparisons, neglecting the fact that these pairs share common operands. Specifically, pair-level methods are prone to the "hubness" trap: they tend to repeatedly query pairs involving the same ambiguous graph (e.g., $\{(G^a, G^1), (G^a, G^2), \dots\}$) simply because G^a itself is hard to characterize. This results in information redundancy concentrated on narrow local regions. In contrast, the graph-centric approach treats selected graphs as anchors. By systematically evaluating an anchor against the population, we acquire a holistic profile of its position in the metric space, rather than merely resolving individual ambiguities. This fosters a more efficient coverage of the global similarity landscape. Empirical validation of this hypothesis is provided in Section 5.

4 Methodology

This section details the EVGS framework, which integrates robust uncertainty quantification with graph-centric querying. We propose a regularized evidential regression mechanism enhanced with a gradient-anchoring term to ensure reliable uncertainty estimation. Based on this, we leverage the estimated uncertainty to select informative graphs, thereby maximizing information gain within the learned metric space.

4.1 Uncertainty Estimation via Regularized Evidential Regression

4.1.1 Probabilistic Modeling via Evidential Regression

Evidential Regression. Standard GSL models typically output deterministic similarity scores, thereby failing to capture the uncertainty estimates crucial for AL. While Bayesian approaches like MC-Dropout (Gal & Ghahramani, 2016) or Deep Ensembles (Lakshminarayanan et al., 2017) can provide such estimates, they often incur high computational costs or memory overheads and yield only coarse approximations. To achieve both reliability and efficiency, we adopt Evidential Regression (Amini et al., 2020). This framework enables uncertainty quantification within a single forward pass by modeling the target as the hyperparameters of a higher-order evidential distribution, which naturally supports uncertainty decomposition.

Formally, rather than modeling the generative process of the graphs themselves, we treat the continuous scalar similarity score $y \in \mathbb{R}$ between a graph pair (G, G') as a sample drawn from a Gaussian distribution with an unknown mean μ and variance σ^2. To capture the uncertainty governing these parameters, we place a Normal-Inverse-Gamma (NIG) conjugate prior over them (Wu et al., 2024; Ye et al., 2024):

$$y \sim \mathcal{N}(\mu, \sigma^2), \quad (\mu, \sigma^2) \sim \mathrm{NIG}(\gamma, \nu, \alpha, \beta) \triangleq \mathcal{N}\left(\mu \mid \gamma, \frac{\sigma^2}{\nu}\right) \Gamma^{-1}(\sigma^2 \mid \alpha, \beta), \tag{2}$$

where Γ^{-1} denotes the inverse-gamma distribution. In this formulation, $\gamma \in \mathbb{R}$ represents the estimated similarity score, $\nu > 0$ quantifies the "predicted evidence" supporting the mean, while $\alpha > 1$ and $\beta > 0$ govern the scale and shape of the variance distribution.

To implement this, we introduce a minimal modification to the GSL backbone. Specifically, we replace the final projection layer with a prediction head that outputs the four hyperparameters $\mathbf{o} = \{\gamma, \nu, \alpha, \beta\}$. This design incurs negligible computational overhead while enabling comprehensive uncertainty quantification.

Uncertainty Decomposition. A key advantage of this framework is the analytical decomposition of uncertainty. Based on the predicted moments of the NIG distribution, we can derive the prediction $\hat{y}$, aleatoric uncertainty $\mathcal{U}_{\text{ale}}$, and epistemic uncertainty $\mathcal{U}_{\text{epi}}$ as follows:

$$\underbrace{\hat{y} = \mathbb{E}[\mu] = \gamma}_{\text{Prediction}}, \quad \underbrace{\mathcal{U}_{\text{ale}} = \mathbb{E}[\sigma^2] = \frac{\beta}{\alpha - 1}}_{\text{Aleatoric Uncertainty}}, \quad \underbrace{\mathcal{U}_{\text{epi}} = \mathrm{Var}[\mu] = \frac{\beta}{\nu(\alpha - 1)}}_{\text{Epistemic Uncertainty}}. \tag{3}$$

We provide the detailed step-by-step mathematical derivation of these uncertainty components in Appendix A.1. Crucially, this decomposition disentangles data-inherent noise ($\mathcal{U}_{\text{ale}}$) from model ignorance ($\mathcal{U}_{\text{epi}}$). In the context of AL, this distinction is paramount. Aleatoric uncertainty arises from the natural complexity or noise within the data distribution and is theoretically irreducible. In contrast, epistemic uncertainty reflects the model's lack of knowledge due to data scarcity. Since the objective of AL is to reduce ignorance, querying instances dominated by high aleatoric uncertainty is inefficient (Park et al., 2023). Accordingly, we formally define our uncertainty metric exclusively based on the epistemic component $\mathcal{U}_{\text{epi}}$.

4.1.2 Optimization Objective and the Proposed Regularization

The Standard Evidential Objective. Following the evidential regression framework, we optimize the model by maximizing the marginal likelihood. Let $\mathbf{o} = \{\gamma, \nu, \alpha, \beta\}$ denote the predicted evidential parameters for a given graph pair with ground-truth similarity y. The marginal likelihood $p(y|\mathbf{o})$ is obtained by

integrating out the latent Gaussian parameters (μ, σ^2):

$$p(y|\mathbf{o}) = \int_{\sigma^2=0}^{\sigma^2=\infty} \int_{\mu=-\infty}^{\mu=\infty} p\left(y|\mu,\sigma^2\right) p\left(\mu,\sigma^2|\mathbf{o}\right) d\mu d\sigma^2 = \mathrm{St}\left(y;\gamma,\frac{\beta(1+\nu)}{\nu\alpha},2\alpha\right). \tag{4}$$

The complete derivation of this marginalization is detailed in Appendix A.2. This integration yields a Student-t distribution $\mathrm{St}(\cdot)$ with location γ, scale $\frac{\beta(1+\nu)}{\nu\alpha}$, and 2α degrees of freedom. Consequently, the primary learning objective is to minimize the Negative Log-Likelihood (NLL):

$$\mathcal{L}_{\mathrm{NLL}} = -\log(p(y|\mathbf{o})) = \frac{1}{2}\log\left(\frac{\pi}{\nu}\right) - \alpha\log(\Omega) + \left(\alpha+\frac{1}{2}\right)\log\left((y-\gamma)^2\nu+\Omega\right) + \log\left(\frac{\Gamma(\alpha)}{\Gamma\left(\alpha+\frac{1}{2}\right)}\right), \tag{5}$$

where $\Gamma(\cdot)$ is the Gamma function and $\Omega = 2\beta(1+\nu)$.

In standard evidential regression (Amini et al., 2020), this objective is typically augmented with a heuristic regularizer, $\mathcal{L}_{\mathrm{REG}}$, designed to constrain the evidence accumulation process:

$$\mathcal{L}_{\mathrm{REG}} = |y-\gamma| \cdot (2\nu+\alpha). \tag{6}$$

Thus, the base objective is formulated as $\mathcal{L}_{\mathrm{base}} = \mathcal{L}_{\mathrm{NLL}} + \lambda\mathcal{L}_{\mathrm{REG}}$, where λ is a balancing coefficient.

The Low-Evidence Trap in Active Learning. While theoretically sound, the evidential objective exhibits a critical pathology, particularly during the early stages of AL when labeled data is scarce. Let us examine the gradient of the dominant term, $\mathcal{L}_{\mathrm{NLL}}$, with respect to the prediction γ:

$$\frac{\partial\mathcal{L}_{\mathrm{NLL}}}{\partial\gamma} = \frac{(2\alpha+1)(y-\gamma)\nu}{(y-\gamma)^2\nu+2\beta(1+\nu)}. \tag{7}$$

We observe that the gradient magnitude is proportional to the evidence ν. In the low-data regime characteristic of early AL cycles, the model tends to predict low evidence (i.e., $\nu \to 0^+$). Consequently, the gradient $\frac{\partial\mathcal{L}_{\mathrm{NLL}}}{\partial\gamma}$ vanishes, regardless of the magnitude of the prediction error. This creates a generic optimization trap: the model can trivially minimize the NLL by simply predicting zero evidence for all samples.

This phenomenon is catastrophic for our AL framework. The query strategy in EVGS relies on relative differences in epistemic uncertainty $\mathcal{U}_{\mathrm{epi}}$ (which is inversely proportional to ν) to distinguish valuable instances. When the model falls into this low-evidence trap, it assigns uniformly high uncertainty to the entire unlabeled pool. This flattens the acquisition landscape, rendering the selection strategy effectively equivalent to random sampling and hindering the model's iterative improvement.

One might expect the standard regularizer, $\mathcal{L}_{\mathrm{REG}}$, to alleviate this issue by providing auxiliary gradients. However, this mechanism is fundamentally misaligned with AL's needs in the low-data regime. First, the gradient signal from $\mathcal{L}_{\mathrm{REG}}$ scales with the evidence magnitude (Oh & Shin, 2022); thus, in the "uniform ignorance" state ($\nu \to 0^+$), the corrective signal effectively vanishes. Second, and more critically, $\mathcal{L}_{\mathrm{REG}}$ is designed to penalize overconfidence on errors (Amini et al., 2020), not to encourage evidence accumulation. Paradoxically, this incentivizes the model to further suppress evidence (reducing ν) to minimize the regularization penalty. Instead of restoring the discriminative uncertainty landscape required for effective sample ranking, standard regularization can inadvertently exacerbate the collapse into a flat, uninformative state.

MSE as a Gradient Anchor for Uncertainty Estimation. To counteract the vanishing gradient problem, we explicitly introduce a Mean Squared Error (MSE) term to anchor the optimization:

$$\mathcal{L}_{\mathrm{MSE}} = (y-\gamma)^2. \tag{8}$$

Crucially, the gradient $\frac{\partial\mathcal{L}_{\mathrm{MSE}}}{\partial\gamma} = 2(\gamma-y)$ is independent of the evidence ν. This term serves as a consistent "gradient injection", ensuring that the model receives robust updates for the target parameter even when it falls into the low-evidence trap ($\nu \to 0^+$). This prevents the model from minimizing the NLL objective by simply outputting "uniform ignorance" to mask prediction errors. Consequently, the epistemic uncertainty

Algorithm 1: Evidential Variance for Graph Selection (EVGS)

Input: Seed labeled set $\mathbb{L}_0$, Unlabeled set $\mathbb{U}_0$, Candidate graph pool $\mathcal{G}_{\text{pool}}$, Graph budget m per cycle, Max active learning cycles T, Reference graph set size K, Hyperparameters λ_1 and λ_2.

Output: Trained GSL model f.

for *cycle* $t = 1$ *to* T **do**

  `// Phase 1: Robust GSL Backbone Training`

  Train f on $\mathbb{L}_{t-1}$ by minimizing the total objective: $\mathcal{L}_{\text{TOTAL}} = \mathcal{L}_{\text{NLL}} + \lambda_1 \mathcal{L}_{\text{REG}} + \lambda_2 \mathcal{L}_{\text{MSE}}$;

  `// Phase 2: Variance-based Graph Selection`

  Initialize scores $\mathbb{S} = \emptyset$;

  for *each candidate graph* $G^i \in \mathcal{G}_{pool}$ **do**

    Sample a random reference subset $\mathcal{S}_i \subseteq \mathcal{G}_{\text{pool}}$ of size K;

    Compute epistemic uncertainty $\mathcal{U}_{\text{epi}}^{ij}$ for all pairs $\{(G^i, G^j) \mid G^j \in \mathcal{S}_i\}$;

    Calculate selection score via uncertainty variance: $s^i = \text{Var}\left\{\mathcal{U}_{\text{epi}}^{ij} \mid G^j \in \mathcal{S}_i\right\}$;

    $\mathbb{S} \leftarrow \mathbb{S} \cup \{s^i\}$;

  Select m graphs corresponding to the highest scores in $\mathbb{S}$, obtaining $\mathcal{G}_t$;

  Generate the query pair batch Δ_t by forming all pairwise constraints within $\mathcal{G}_t$;

  `// Phase 3: Update`

  Query labels for Δ_t and update sets:

  $\mathbb{L}_t \leftarrow \mathbb{L}_{t-1} \cup \Delta_t,\ \mathbb{U}_t \leftarrow \mathbb{U}_{t-1} \setminus \Delta_t,\ \mathcal{G}_{\text{pool}} \leftarrow \mathcal{G}_{\text{pool}} \setminus \mathcal{G}_t$;

return f

derived from the evidential parameters is forced to reflect actual data density rather than optimization failures, thereby restoring the discriminative landscape necessary for effective AL queries.

Combining these components, the training objective in our EVGS framework, $\mathcal{L}_{\text{TOTAL}}$, is defined as:

$$\mathcal{L}_{\text{TOTAL}} = \mathcal{L}_{\text{NLL}} + \lambda_1 \mathcal{L}_{\text{REG}} + \lambda_2 \mathcal{L}_{\text{MSE}}, \tag{9}$$

where λ_1 and λ_2 are hyperparameters balancing the regularization strength and the gradient-anchoring effect, respectively. In this composite framework, $\mathcal{L}_{\text{NLL}}$ drives the learning of the evidential distribution, $\mathcal{L}_{\text{REG}}$ penalizes overconfidence on outliers, and $\mathcal{L}_{\text{MSE}}$ ensures continuous gradient flow to prevent evidence collapse, collectively enabling robust uncertainty estimation for AL.

4.2 Graph-Centric Selection via Uncertainty Variance

While conventional AL strategies prioritize instances with maximal epistemic uncertainty, applying this naively to GSL is suboptimal due to the combinatorial nature of the input space. A purely pairwise perspective is structurally myopic: it treats comparisons as isolated events, ignoring that they share common constituent graphs. This often leads to the "hubness" trap, where the model redundantly queries multiple pairs involving the same ambiguous graph, yielding diminishing returns. To overcome this, we adopt a graph-centric strategy. By evaluating how a graph interacts with the population, we capture its holistic position in the metric space rather than merely resolving local ambiguities.

To implement this graph-centric perspective, we propose that the informativeness of a graph G^i is effectively captured by the variability of the model's uncertainty regarding it. Intuitively, if a graph lies in a well-learned region, the model should exhibit consistently low uncertainty across comparisons; conversely, if a graph is a "hard" sample, uncertainty tends to be consistently high. The most valuable instances are those situated in ambiguous regions of the metric space, where the model's epistemic uncertainty fluctuates significantly.

Formally, for each candidate graph G^i in the pool $\mathcal{G}_{\text{pool}}$, we quantify this fluctuation by measuring the variance of its epistemic uncertainty. To circumvent the prohibitive $O(N^2)$ computational cost of exhaustive pairing ($N = |\mathcal{G}_{\text{pool}}|$), we employ a stochastic approximation. Specifically, for each G^i, we sample a random reference subset $\mathcal{S}_i \subseteq \mathcal{G}_{\text{pool}}$ of size K ($K \ll N$). This approximation reduces the selection complexity from

quadratic to linear $O(NK)$, ensuring scalability for large-scale datasets. The selection score s^i is defined as:

$$s^i = \mathrm{Var}\left\{\mathcal{U}_{\mathrm{epi}}^{ij} \mid G^j \in \mathcal{S}_i\right\}. \tag{10}$$

We prioritize variance over conventional mean uncertainty to explicitly target relational ambiguity rather than inherent difficulty. A graph with consistently high uncertainty (high mean, low variance) often indicates an instance with unique substructures that the model struggles to match against references. While difficult, such graphs may be plagued by irreducible noise or domain shifts, yielding diminishing returns for the active learner. From a generalization perspective, targeting these high-variance instances stabilizes the global metric structure. Since GSL aims to approximate a smooth similarity manifold, graphs exhibiting erratic confidence fluctuations act as local "singularities" that disrupt this smoothness. Annotating these instances compels the model to resolve such inconsistencies, effectively "pinning" the embedding of G^i to a stable location that satisfies relational constraints. This resolves topological ambiguities and facilitates more effective gradient propagation throughout the similarity network.

Putting this into practice, the complete EVGS workflow is outlined in Algorithm 1. The process alternates between optimizing the evidential GSL model with our MSE-anchored objective ($\mathcal{L}_{\mathrm{TOTAL}}$) and selecting instances via the stochastic variance score (s^i). This iterative loop ensures that the model stabilizes regions with inconsistent labels while maintaining robust gradient signals throughout the active learning lifecycle.

4.3 Discussions

While EVGS builds upon established concepts such as evidential learning and uncertainty sampling, its true value lies in how it adapts and synergizes these elements to solve fundamentally new bottlenecks in active learning for graph similarity learning. To distinguish our framework from a straightforward combination of existing techniques, we highlight our core innovations across three perspectives:

Task Perspective (Bridging AL and GSL). EVGS pioneers the integration of AL into GSL. Unlike traditional graph AL, which predominantly focuses on discrete node classification, we identify two unique challenges inherent to this novel setting: (1) *Uncertainty Quantification in Regression* and (2) *Structural Dependency in Paired Inputs*. By formalizing this new paradigm and addressing these challenges, EVGS provides a foundational framework that benefits both the AL and graph representation learning communities.

Methodological Perspective (Adapting Evidential Regression for AL). To address the first challenge, we move beyond computationally prohibitive estimators by adapting Evidential Regression for AL. Crucially, EVGS is not a mere plug-and-play application. We uncover a fundamental limitation of evidential models: severe uncertainty degradation, specifically in *low-data AL regimes*, and introduce a targeted regularization strategy. This methodological refinement ensures robust uncertainty quantification for AL.

Algorithmic Philosophy (Graph-centric vs. Pair-level). To overcome the second challenge, we break away from the standard AL assumption of instance independence. We expose the "Hubness" trap inherent in naive pair-level sampling, in which independently selecting high-uncertainty pairs leads to severe structural redundancy. As a philosophical shift, EVGS introduces a *graph-centric* acquisition strategy based on uncertainty variance. By explicitly modeling the variance and structural interactions among candidate pairs, our approach transitions AL from isolated instance selection to holistic graph sampling.

5 Experiments

5.1 Experimental Settings

Datasets. We evaluate EVGS on three widely recognized benchmarks: AIDS (Liang & Zhao, 2017), LINUX (Wang et al., 2012), and IMDB (Yanardag & Vishwanathan, 2015). These datasets span diverse domains, representing chemical compounds, program dependency graphs, and social interaction networks. Following standard protocols, we adopt a random 60%/20%/20% split for training, validation, and testing.

Datasets	Full Statistics		Initial Seed Set ($t = 0$)		Active Query Batch ($t > 0$)	
	# Graphs	# Pairs	# Graphs ($\|\mathcal{G}_0\|$)	# Pairs ($\|\mathbb{L}_0\|$)	# Graphs (m)	# Pairs ($\|\Delta_t\|$)
AIDS	700	244,650	70	2,415	35	595
LINUX	1,000	499,500	100	4,950	50	1,225
IMDB	1,500	1,124,250	150	11,175	75	2,775

Table 1: Statistical summary and active learning configurations of used datasets.

Active Learning Protocols. We initialize the training process by randomly sampling a seed set of graphs $\mathcal{G}_0$ from each dataset. To construct the initial labeled pool $\mathbb{L}_0$, we generate a fully connected graph of constraints, pairing all instances within $\mathcal{G}_0$. Consequently, the initial labeled set size is $|\mathbb{L}_0| = \binom{|\mathcal{G}_0|}{2}$. Specifically, we set $|\mathcal{G}_0|$ to 70, 100, and 150 for AIDS, LINUX, and IMDB, respectively. This results in 2,415, 4,950, and 11,175 initial pairs, accounting for less than 1.0% of the total possible pairs. The AL process spans 18 iterations. In each iteration t, after training the model to convergence on $\mathbb{L}_{t-1}$, we select m informative graphs using our graph-centric strategy. To maintain consistency with the initialization phase, the incremental labeled set Δ_t is formed by densely pairing graphs within the selected batch $\mathcal{G}_t$. This yields $|\Delta_t| = \binom{m}{2}$ new labeled pairs per round. We set m to 35, 50, and 75 for the three datasets, corresponding to 595, 1,225, and 2,775 new pairs per iteration. For a fair comparison with baselines that employ pair-level query strategies, we strictly control the budget by selecting exactly $|\Delta_t|$ pairs. This configuration demonstrates high data efficiency: even after 18 iterations, the cumulative labeled pairs remain below 5.5% of the total available pairs. Table 1 provides a comprehensive summary of these statistics.

Metrics. Following standard GSL protocols (Bai et al., 2019; Tan et al., 2023), we evaluate performance using three key metrics: Mean Squared Error (MSE) for regression accuracy, Spearman's Rank Correlation Coefficient (ρ) (Spearman, 1904) for ranking consistency, and Precision at 10 (P@10) for search quality.

GSL Backbones. To validate the model-agnostic nature of EVGS, we instantiate it with two representative backbones featuring distinct paradigms: the histogram-aggregation-based SimGNN (Bai et al., 2019) and the attention-aggregation-based NA-GSL (Tan et al., 2023). This diversity allows us to verify the framework's generalizability across different architectural strategies.

Implementation Details. We implement EVGS using PyTorch Geometric 2.4.0 on an NVIDIA RTX 3080 GPU. To ensure fair comparison, we strictly adhere to the original architectural settings for the SimGNN (Bai et al., 2019) and NA-GSL (Tan et al., 2023) backbones. All models are optimized via Adam (learning rate = 0.001, batch size = 128). Regarding EVGS-specific hyperparameters, we set the balancing coefficients $\lambda_1 = 0.01$ and $\lambda_2 = 0.1$ in equation 9 based on a grid search. The reference subset size is fixed at $K = 10$ to balance efficiency and estimation accuracy; detailed sensitivity analyses are provided in the Appendix B.1. Finally, we report the mean performance over 5 independent runs, with standard deviations visualized as shaded regions. Source code is available at `https://anonymous.4open.science/r/TMLR-EVGS`.

5.2 Performance Evaluation

5.2.1 Analysis on Query Strategies: Pairs vs. Graphs

To validate the superiority of our graph-centric variance-based selection, we conduct an ablation study using SimGNN on the AIDS dataset. We compare EVGS against two variants: **(1) EPS (Evidential Pair Selection)**, a pair-level strategy that directly selects pairs with the highest epistemic uncertainty $\mathcal{U}_{\text{epi}}$; and **(2) EMGS (Evidential Mean for Graph Selection)**, a graph-centric strategy that selects graphs maximizing the *mean* uncertainty of their associated pairs, rather than the variance.

As shown in Figures 1(a)-1(c), EPS consistently underperforms EVGS. Figure 1(d) reveals the underlying cause via t-SNE visualization: EPS suffers from a "hub effect." By myopically focusing on high-uncertainty pairs, it repeatedly samples pairs connected to the same "hub" graphs. Quantitatively, despite a budget of

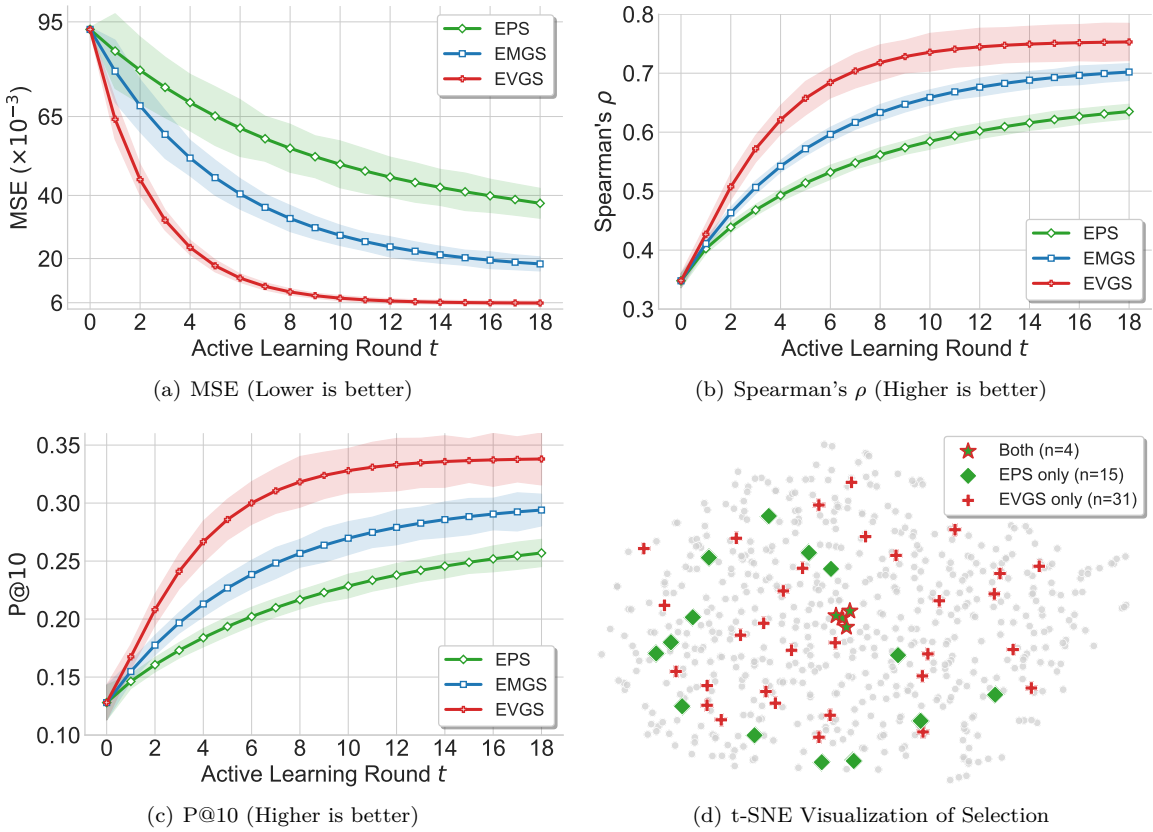

(a) MSE (Lower is better)

(b) Spearman's ρ (Higher is better)

(c) P@10 (Higher is better)

(d) t-SNE Visualization of Selection

Figure 1: **Ablation study on query strategies** using SimGNN on the AIDS dataset.

35 graphs, EPS yields only **19 unique graphs**, resulting in redundant coverage and a failure to explore the broader data manifold. In contrast, EVGS explicitly optimizes for graph diversity, ensuring a uniform span of the similarity space. This demonstrates that treating pairs as independent atomic units is suboptimal; instead, graph-centric selection is essential to maximize the marginal information gain of each query.

These results also show that *variance* (EVGS) consistently outperforms the *mean* (EMGS). While EMGS prioritizes graphs exhibiting consistently high uncertainty across all pairings, our analysis suggests these often correspond to samples with inherently ambiguous substructures. The uncertainty associated with such samples is likely irreducible, implying that querying them yields diminishing returns. In contrast, EVGS targets graphs with high variance, identifying instances where the model is confident in some contexts but ambiguous in others. This high variance indicates that the graph lies in a transition region of the metric space, where the learned similarity function is most sensitive to perturbations. By labeling these pivotal instances, EVGS effectively refines the local geometry of the embedding manifold, thereby improving generalization.

5.2.2 Impact of Uncertainty Quantification Mechanisms

To validate the efficacy of our evidential regression framework and its components, we conduct an ablation study using NA-GSL on the LINUX dataset. We compare EVGS against two categories of variants:

(1) External Uncertainty Baselines. We replace our evidential framework with established uncertainty estimation methods while keeping the graph-centric selection strategy:

- **MVGS (MC-Dropout):** Estimates uncertainty via prediction variance over 25 stochastic forward passes (Gal & Ghahramani, 2016; Beluch et al., 2018).

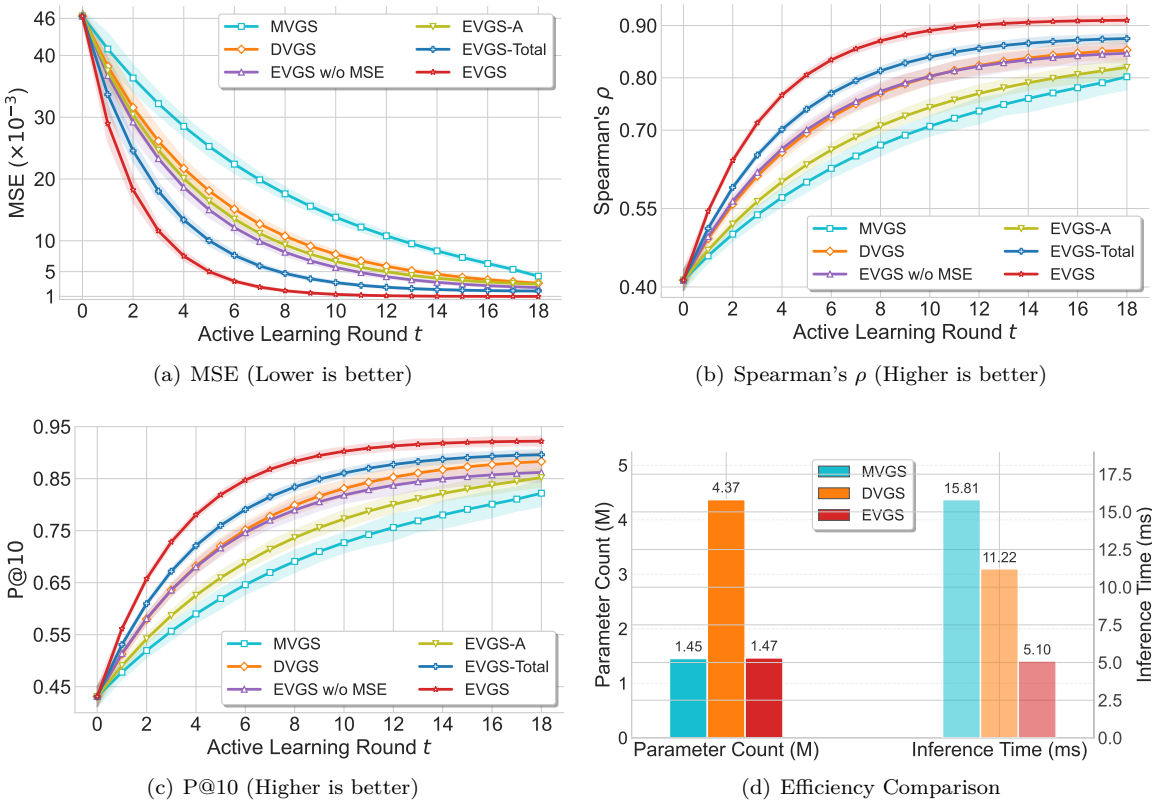

(a) MSE (Lower is better)

(b) Spearman's ρ (Higher is better)

(c) P@10 (Higher is better)

(d) Efficiency Comparison

Figure 2: **Ablation study on uncertainty quantification** using NA-GSL on the LINUX dataset.

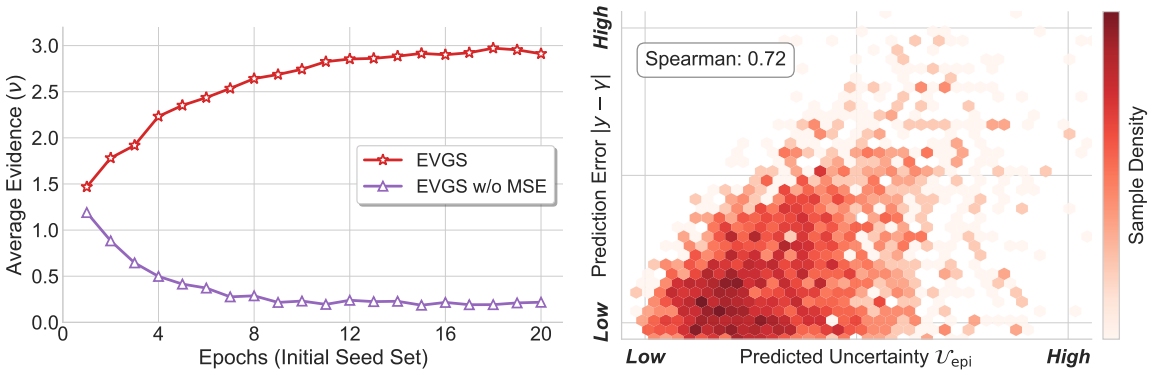

(a) Evolution of ν

(b) Uncertainty vs. Error

Figure 3: Empirical analysis of EVGS in **(a) training stability** and **(b) uncertainty estimation**.

- **DVGS (Deep Ensemble):** Estimates uncertainty using an ensemble of 3 independently trained models (Lakshminarayanan et al., 2017; Choi et al., 2021).

(2) Internal Ablations. We evaluate specific loss terms and uncertainty metrics within EVGS:

- **EVGS w/o MSE:** Removes loss term $\mathcal{L}_{\text{MSE}}$ to isolate the effect of the proposed regularization.
- **EVGS-A (Aleatoric):** Selects graphs based on aleatoric uncertainty ($\mathcal{U}_{\text{ale}}$).
- **EVGS-Total:** Uses total uncertainty ($\mathcal{U}_{\text{total}} = \mathcal{U}_{\text{ale}} + \mathcal{U}_{\text{epi}}$) as the selection metric.

As shown in Figures 2(a)-2(c), EVGS consistently outperforms all variants. First, the inferior performance of EVGS-A validates our premise: aleatoric uncertainty reflects inherent data noise rather than epistemic ignorance. In an AL context, querying samples with high aleatoric uncertainty is inefficient, as the budget is squandered on irreducible noise rather than learnable structures. Consequently, EVGS-Total also degrades due to contamination from this noise component. Second, the performance drop in EVGS w/o MSE underscores the necessity of the regularization term. To explicitly demonstrate its internal mechanism, we track the average predicted evidence (ν) during the initial training phase on the seed set (Figure 3(a)). As observed, without the MSE anchor, the evidential model quickly falls into a "low-evidence trap" where ν collapses to near zero. As theoretically derived in Section 4.1.2, the gradient of the NLL loss with respect to the predictive mean γ is directly proportional to the evidence (i.e., $\frac{\partial \mathcal{L}_{\text{NLL}}}{\partial \gamma} \propto \nu$). Consequently, this collapse of ν mathematically forces these specific gradients to vanish, halting the learning process of the target variable right from the start. Such an early failure is fatal, as it permanently derails the model's optimization and severely degrades all subsequent AL cycles. In contrast, including the MSE anchor effectively maintains a healthy level of evidence, preventing vanishing gradients and ensuring stable optimization. Furthermore, to verify that the well-trained EVGS model produces reliable uncertainty estimates, we visualize the relationship between the predicted epistemic uncertainty ($\mathcal{U}_{\text{epi}}$) and the absolute prediction error ($|y - \gamma|$) in Figure 3(b). The clear positive correlation visually confirms that $\mathcal{U}_{\text{epi}}$ accurately reflects the model's true ignorance. In our graph-centric active learning framework, this reliability is paramount: it ensures that the uncertainty-derived scores (i.e., the variance of uncertainty) faithfully represent the actual error distribution across the graph, firmly justifying $\mathcal{U}_{\text{epi}}$ as a robust foundation for our acquisition metric.

Compared to external baselines, EVGS demonstrates superior efficacy and performance by addressing fundamental theoretical and computational limitations. Theoretically, MVGS and DVGS typically conflate aleatoric and epistemic uncertainties into a single predictive variance, lacking the granularity to filter out noisy samples. In contrast, EVGS leverages a higher-order conjugate prior to explicitly disentangle epistemic uncertainty within a single forward pass. Computationally, as shown in Figure 2(d), EVGS avoids the substantial parameter overhead of ensembles (DVGS) and the inference latency of stochastic sampling (MVGS). This establishes EVGS as a uniquely efficient solution for active graph similarity learning, delivering precise uncertainty estimation without incurring prohibitive resource costs.

5.2.3 Comparison with Baselines

Baselines. Given the scarcity of dedicated AL methods for graph similarity, we adapt representative strategies to this setting. Where applicable, we evaluate two variants: *Pair-level (P)*, operating on the joint pair embedding $\mathbf{z}$, and *Graph-centric (G)*, operating on individual graph embeddings $\mathbf{g}$.

- **Random:** Uniformly selects samples from the unlabeled pool. We report a unified baseline, as empirical results showed negligible differences between random-pair and random-graph selection.
- **Coreset (Sener & Savarese, 2018):** A diversity-based approach using k-Center Greedy ($k = 4$) to minimize the covering radius of the labeled set. We implement both **Coreset-P** and **Coreset-G**.
- **Cluster (Nguyen & Smeulders, 2004):** A density-based strategy using k-means ($k = 4$) to select representative instances near centroids. We evaluate both **Cluster-P** and **Cluster-G**.
- **BADGE (Ash et al., 2020):** A hybrid strategy that clusters samples in the gradient space to capture uncertainty and diversity. Inherently pair-centric, as gradients derive from the pairwise loss.

Figure 4 reports the AL performance on the IMDB dataset (additional datasets are detailed in Appendix B.2). Our proposed EVGS consistently outperforms all baselines across all metrics and backbones. Notably, EVGS exhibits the steepest learning curve in the initial rounds (0-6). For example, as shown in Figure 4(a), it reduces MSE significantly faster than BADGE and Coreset-G, demonstrating that evidential variance effectively identifies informative graphs for rapid adaptation. Furthermore, the narrow confidence intervals of EVGS indicate greater stability than the high variance observed in Random and Cluster-based methods.

The consistent superiority of graph-centric variants validates our hypothesis and the analysis in Section 5.2.1. This confirms that redundancy primarily stems from graph structures, where selecting diverse individual graphs implicitly covers the interaction space more efficiently than pair-based selection.

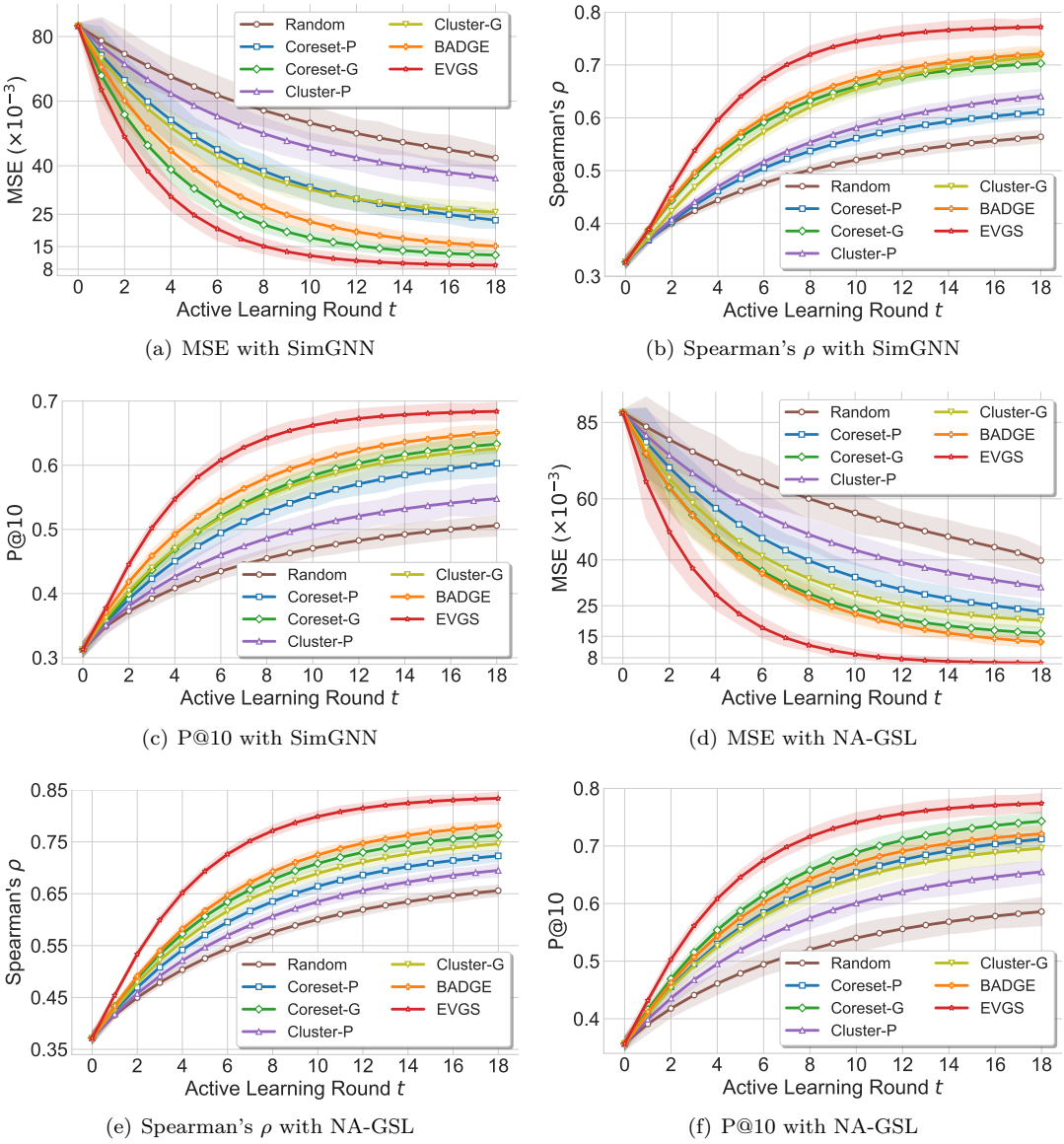

(a) MSE with SimGNN

(b) Spearman's ρ with SimGNN

(c) P@10 with SimGNN

(d) MSE with NA-GSL

(e) Spearman's ρ with NA-GSL

(f) P@10 with NA-GSL

Figure 4: **Performance comparison with baselines** on the IMDB dataset.

To assess data efficiency, we compare EVGS at the final round (utilizing merely 5.5% of the training pairs) against the Full-Data baseline. On IMDB with SimGNN, the Full-Data model achieves an MSE of 1.264×10^{-3}. Remarkably, despite a $\approx 95\%$ reduction in annotation cost, EVGS achieves an MSE of 9.236×10^{-3}, successfully maintaining the same order of magnitude as the full-data result. Furthermore, it retains 87.9% of the rank correlation ($\rho = 0.772$) and 90.1% of the retrieval precision (P@10 $= 0.684$). These results demonstrate that EVGS can achieve prediction errors comparable to those of fully supervised approaches, confirming its ability to identify the minimal informative subset necessary for generalization.

5.3 In-depth Analysis of EVGS

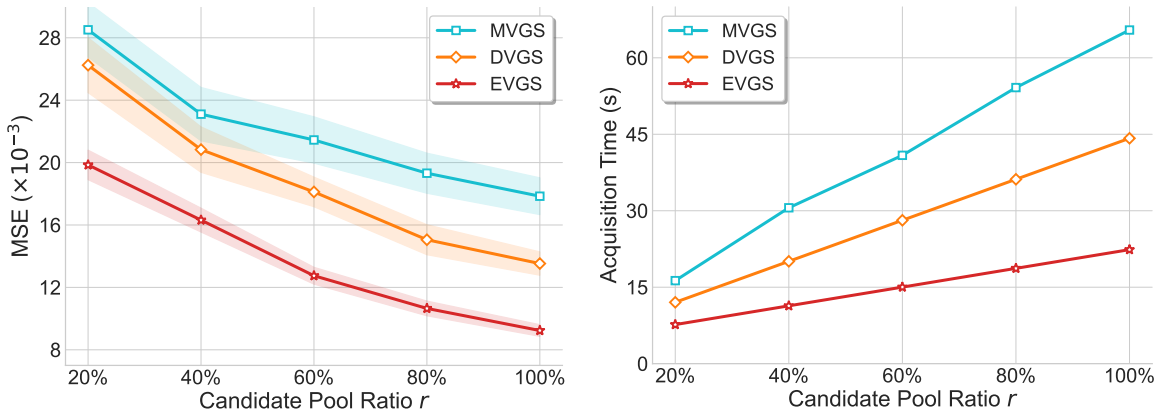

(a) Performance Robustness

(b) Acquisition Time Efficiency

Figure 5: **Scalability analysis of EVGS**: (a) performance and (b) efficiency.

5.3.1 Scalability of EVGS

To evaluate the scalability of EVGS in real-world large-scale scenarios, we conduct an in-depth analysis on the IMDB dataset. We design a "Controlled Pool Expansion" experiment to investigate how different selection strategies scale with an increasing number of candidate graphs. Specifically, during the acquisition phase, we artificially restrict the available unlabeled pool to proportions $r \in \{20\%, 40\%, 60\%, 80\%, 100\%\}$. We compare EVGS with two strong uncertainty-based baselines: MVGS (MC-Dropout) and DVGS (Deep Ensembles). The evaluation focuses on two critical dimensions: predictive performance (measured by the final MSE) and computational efficiency (measured by the acquisition time per round).

First, regarding *algorithmic scalability* (Figure 5(a)), we observe that as the candidate pool ratio r increases, the MSE of all methods decreases, as a larger pool provides a broader search space for informative samples. However, EVGS consistently maintains the lowest MSE across all pool sizes. This demonstrates that our acquisition metric effectively leverages the expanded search space to pinpoint highly valuable graphs, rather than being distracted by the growing number of redundant or noisy candidates in a massive pool.

Second, regarding *computational scalability* (Figure 5(b)), EVGS exhibits an overwhelming advantage in time efficiency. Naturally, as the candidate pool size grows, the acquisition time for all methods increases. However, traditional uncertainty estimation methods such as MVGS and DVGS require multiple forward passes per graph pair, leading to remarkably steep slopes. In stark contrast, EVGS derives predictive uncertainty analytically via a *single forward pass* within the Evidential Regression framework. Consequently, its time cost scales with an extremely flat slope. This "fan-shaped" divergence in acquisition time confirms that EVGS is highly scalable and exceptionally well-suited for massive graph datasets.

Third, regarding *graph-size scalability*, it is crucial to note that while our graph-centric selection successfully reduces the combinatorial complexity from $O(N^2)$ to $O(NK)$ concerning the number of graphs, the computational cost of evaluating a single pair remains dependent on the size of the graphs (i.e., the number of nodes and edges). We emphasize that this node/edge-level complexity is inherently tied to the underlying GSL architecture rather than the EVGS framework itself. Because EVGS is strictly backbone-agnostic, it can smoothly scale to datasets with massive graphs by employing lightweight, embedding-based GSL models (which compute graph-level embeddings independently prior to a simple distance metric) instead of computationally heavy interaction-based models (e.g., those relying on dense cross-graph attention). Consequently, EVGS serves as a highly flexible meta-framework, allowing practitioners to explicitly trade off between pair-level inference latency and representation expressiveness based on their specific graph dimensions.

5.3.2 Analysis of Selected Graphs

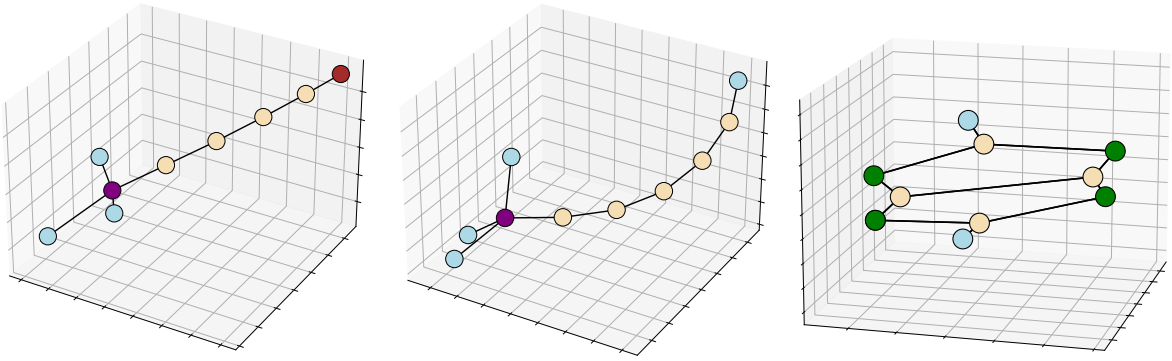

(a) Graph-117 (b) Graph-126 (c) Graph-129

Figure 6: **Visualization of representative graphs selected by EVGS.**

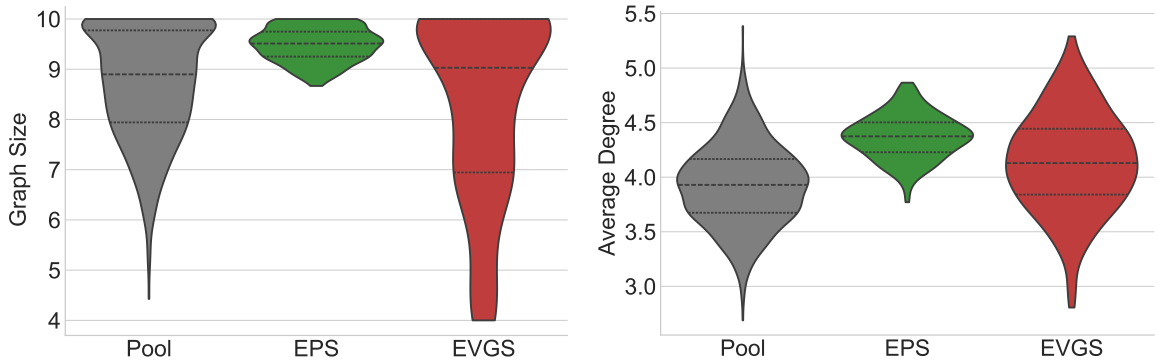

(a) Distribution of Graph Size (b) Distribution of Average Degree

Figure 7: Distributions of **(a) graph size** and **(b) average degree** for the selected graph subsets.

To provide qualitative insight into the efficacy of our graph-centric strategy, Figure 6 visualizes representative graphs selected by EVGS. Driven by our evidential variance metric, the selected subset exhibits significant topological diversity. This graph-centric diversity naturally yields training pairs spanning a broad spectrum of ground-truth similarities. For example, the selected pool contains graphs that form highly structurally isomorphic pairs (e.g., Figure 6(a) and Figure 6(b)) as well as structurally distinct pairs (e.g., Figure 6(b) and Figure 6(c)). This diversity is instrumental for efficient model training in two critical aspects:

- **Metric Calibration via Anchors:** By querying pairs at both ends of the similarity spectrum (i.e., highly similar vs. highly dissimilar), EVGS provides the model with critical "anchors" to calibrate the regression scale. This effectively prevents the model from collapsing into trivial solutions or exhibiting bias towards the mean similarity score.

- **Structural Manifold Coverage:** The distinct topological variations observed in the selected graphs confirm that EVGS effectively explores diverse regions of the graph space. Unlike baselines that suffer from the "hub effect" (i.e., repeatedly selecting a redundant set of certain graphs), our method identifies informative instances that broadly cover the underlying data manifold, thereby accelerating the generalization capability of the GSL backbone.

To empirically validate our analysis regarding the pathological behavior of pair-level selection strategies, we investigate the topological properties of the graph subsets queried by different methods. Specifically, we compare our EVGS against the pair-level strategy (EPS) and the overall data pool. We employ graph size (number of nodes) and average degree as two fundamental proxies for structural complexity.

As illustrated in Figure 7, a stark contrast emerges between the two AL strategies. The subset selected by EPS deviates significantly from the true distribution, heavily concentrating on the upper bounds. This visual evidence perfectly captures the "hubness trap": EPS is easily misled by dense, ambiguous substructures, wasting the query budget on highly redundant, complex graphs. Conversely, our proposed EVGS exhibits a distinct, uniform distribution that spans the entire range of structural metrics, from extremely sparse graphs to dense substructures. Rather than collapsing into local topological traps, EVGS successfully selects a diverse set of graphs that act as *topological anchors*. These phenomena strongly corroborate our motivation: unlike pair-level strategies that are vulnerable to complex topologies, EVGS uniformly covers the structural manifold, thereby providing an unbiased and comprehensive structural calibration for the model.

6 Conclusion

This work pioneers the integration of AL with GSL, establishing a data-efficient paradigm to address the prohibitive annotation costs in GSL. We introduce EVGS, a generalizable framework that overcomes two fundamental challenges: it quantifies regression uncertainty via evidential deep learning with MSE regularization, and resolves the combinatorial complexity of paired inputs through a novel graph-centric selection strategy based on uncertainty variance. Extensive experiments across three benchmarks and two GSL architectures demonstrate that EVGS consistently outperforms established baselines. By shifting the focus from pairwise to graph-centric informativeness, our work offers fresh insights into the structural redundancy in GSL datasets and paves a new avenue for cost-effective graph representation learning.

References

Alexander Amini, Wilko Schwarting, Ava Soleimany, and Daniela Rus. Deep evidential regression. In *Advances in Neural Information Processing Systems*, pp. 14927–14937, 2020.

Jordan T Ash, Chicheng Zhang, Akshay Krishnamurthy, John Langford, and Alekh Agarwal. Deep batch active learning by diverse, uncertain gradient lower bounds. In *International Conference on Learning Representations*, 2020.

Yunsheng Bai, Hao Ding, Song Bian, Ting Chen, Yizhou Sun, and Wei Wang. SimGNN: A neural network approach to fast graph similarity computation. In *Proceedings of the ACM International Conference on Web Search and Data Mining*, pp. 384–392, 2019.

Yunsheng Bai, Hao Ding, Ken Gu, Yizhou Sun, and Wei Wang. Learning-based efficient graph similarity computation via multi-scale convolutional set matching. In *Proceedings of the AAAI Conference on Artificial Intelligence*, pp. 3219–3226, 2020.

William H Beluch, Tim Genewein, Andreas Nürnberger, and Jan M Köhler. The power of ensembles for active learning in image classification. In *IEEE Conference on Computer Vision and Pattern Recognition*, pp. 9368–9377, 2018.

Horst Bunke and Kim Shearer. A graph distance metric based on the maximal common subgraph. *Pattern Recognition Letters*, 19(3-4):255–259, 1998.

Hongyun Cai, Vincent W Zheng, and Kevin Chen-Chuan Chang. Active learning for graph embedding, 2017.

Wenbin Cai, Muhan Zhang, and Ya Zhang. Batch mode active learning for regression with expected model change. *IEEE Transactions on Neural Networks and Learning Systems*, 28(7):1668–1681, 2016.

Xinlong Chen, Mingyu Lin, Yuzhuo Wang, Jin Li, Feiyang Ye, and Yang-Geng Fu. Feature space variation-based active learning sample query strategy for graph deep learning. *Expert Systems with Applications*, 308:131165, 2026.

Jiwoong Choi, Ismail Elezi, Hyuk-Jae Lee, Clement Farabet, and Jose M Alvarez. Active learning for deep object detection via probabilistic modeling. In *IEEE/CVF Conference on Computer Vision and Pattern Recognition*, pp. 10264–10273, 2021.

Limeng Cui, Xianfeng Tang, Sumeet Katariya, Nikhil Rao, Pallav Agrawal, Karthik Subbian, and Dongwon Lee. ALLIE: Active learning on large-scale imbalanced graphs. In *ACM Web Conference*, pp. 690–698, 2022.

Khoa D Doan, Saurav Manchanda, Suchismit Mahapatra, and Chandan K Reddy. Interpretable graph similarity computation via differentiable optimal alignment of node embeddings. In *Proceedings of the International ACM SIGIR Conference on Research and Development in Information Retrieval*, pp. 665–674, 2021.

Yarin Gal and Zoubin Ghahramani. Dropout as a Bayesian approximation: Representing model uncertainty in deep learning. In *International Conference on Machine Learning*, pp. 1050–1059, 2016.

Li Gao, Hong Yang, Chuan Zhou, Jia Wu, Shirui Pan, and Yue Hu. Active discriminative network representation learning. In *Proceedings of the International Joint Conference on Artificial Intelligence*, pp. 2142–2418, 2018.

Xinbo Gao, Bing Xiao, Dacheng Tao, and Xuelong Li. A survey of graph edit distance. *Pattern Analysis and Applications*, 13(1):113–129, 2010.

Sheng Guan, Hanchao Ma, Mengying Wang, and Yinghui Wu. GALE: Active adversarial learning for erroneous node detection in graphs. In *IEEE International Conference on Data Engineering*, pp. 1705–1718, 2023.

Wei Ju, Siyu Yi, Yifan Wang, Zhiping Xiao, Zhengyang Mao, Hourun Li, Yiyang Gu, Yifang Qin, Nan Yin, Senzhang Wang, et al. A survey of graph neural networks in real world: Imbalance, noise, privacy and OOD challenges. *IEEE Transactions on Pattern Analysis and Machine Intelligence*, pp. 1–20, 2025.

Balaji Lakshminarayanan, Alexander Pritzel, and Charles Blundell. Simple and scalable predictive uncertainty estimation using deep ensembles. In *Advances in Neural Information Processing Systems*, pp. 6402–6413, 2017.

Zixun Lan, Binjie Hong, Ye Ma, and Fei Ma. More interpretable graph similarity computation via maximum common subgraph inference. *IEEE Transactions on Knowledge and Data Engineering*, 36(11):6588–6599, 2024.

Qimai Li, Zhichao Han, and Xiao-Ming Wu. Deeper insights into graph convolutional networks for semi-supervised learning. In *Proceedings of the AAAI Conference on Artificial Intelligence*, pp. 1399–1414, 2018.

Yayong Li, Jie Yin, and Ling Chen. SEAL: Semisupervised adversarial active learning on attributed graphs. *IEEE Transactions on Neural Networks and Learning Systems*, 32(7):3136–3147, 2020.

Yujia Li, Chenjie Gu, Thomas Dullien, Oriol Vinyals, and Pushmeet Kohli. Graph matching networks for learning the similarity of graph structured objects. In *International Conference on Machine Learning*, pp. 3835–3845, 2019.

Yongjiang Liang and Peixiang Zhao. Similarity search in graph databases: A multi-layered indexing approach. In *IEEE International Conference on Data Engineering*, pp. 783–794, 2017.

Xiang Ling, Lingfei Wu, Saizhuo Wang, Tengfei Ma, Fangli Xu, Chunming Wu, and Shouling Ji. Hierarchical graph matching networks for deep graph similarity learning, 2019.

Xiang Ling, Lingfei Wu, Saizhuo Wang, Tengfei Ma, Fangli Xu, Alex X Liu, Chunming Wu, and Shouling Ji. Multilevel graph matching networks for deep graph similarity learning. *IEEE Transactions on Neural Networks and Learning Systems*, 34(2):799–813, 2021.

Guixiang Ma, Nesreen K Ahmed, Theodore L Willke, Dipanjan Sengupta, Michael W Cole, Nicholas B Turk-Browne, and Philip S Yu. Deep graph similarity learning for brain data analysis. In *Proceedings of the ACM International Conference on Information and Knowledge Management*, pp. 2743–2751, 2019.

Guixiang Ma, Nesreen K Ahmed, Theodore L Willke, and Philip S Yu. Deep graph similarity learning: A survey. *Data Mining and Knowledge Discovery*, 35(3):688–725, 2021.

Hieu T Nguyen and Arnold Smeulders. Active learning using pre-clustering. In *International Conference on Machine Learning*, pp. 79, 2004.

Giannis Nikolentzos, Polykarpos Meladianos, and Michalis Vazirgiannis. Matching node embeddings for graph similarity. In *Proceedings of the AAAI Conference on Artificial Intelligence*, pp. 2429–2435, 2017.

Dongpin Oh and Bonggun Shin. Improving evidential deep learning via multi-task learning. In *Proceedings of the AAAI Conference on Artificial Intelligence*, pp. 7895–7903, 2022.

Younghyun Park, Wonjeong Choi, Soyeong Kim, Dong-Jun Han, and Jaekyun Moon. Active learning for object detection with evidential deep learning and hierarchical uncertainty aggregation. In *International Conference on Learning Representations*, 2023.

Can Qin, Handong Zhao, Lichen Wang, Huan Wang, Yulun Zhang, and Yun Fu. Slow learning and fast inference: Efficient graph similarity computation via knowledge distillation. In *Advances in Neural Information Processing Systems*, pp. 14110–14121, 2021.

Rishabh Ranjan, Siddharth Grover, Sourav Medya, Venkatesan Chakaravarthy, Yogish Sabharwal, and Sayan Ranu. GREED: A neural framework for learning graph distance functions. In *Advances in Neural Information Processing Systems*, pp. 22518–22530, 2022.

Pengzhen Ren, Yun Xiao, Xiaojun Chang, Po-Yao Huang, Zhihui Li, Brij B Gupta, Xiaojiang Chen, and Xin Wang. A survey of deep active learning. *ACM Computing Surveys*, 54(9):1–40, 2021.

Pau Riba, Andreas Fischer, Josep Lladós, and Alicia Fornés. Learning graph distances with message passing neural networks. In *International Conference on Pattern Recognition*, pp. 2239–2244, 2018.

Ozan Sener and Silvio Savarese. Active learning for convolutional neural networks: A core-set approach. In *International Conference on Learning Representations*, 2018.

Murat Sensoy, Lance Kaplan, and Melih Kandemir. Evidential deep learning to quantify classification uncertainty. In *Advances in Neural Information Processing Systems*, pp. 3183–3193, 2018.

Burr Settles. Active learning literature survey. Technical report, University of Wisconsin-Madison, 2009.

H Sebastian Seung, Manfred Opper, and Haim Sompolinsky. Query by committee. In *Proceedings of the Annual Workshop on Computational Learning Theory*, pp. 287–294, 1992.

Zeang Sheng, Weiyang Guo, Yingxia Shao, Wentao Zhang, and Bin Cui. LLMs are noisy Oracles! LLM-based noise-aware graph active learning for node classification. In *Proceedings of the ACM SIGKDD Conference on Knowledge Discovery and Data Mining*, pp. 2526–2537, 2025.

Alexander Sorokin and David Forsyth. Utility data annotation with Amazon mechanical turk. In *IEEE Computer Society Conference on Computer Vision and Pattern Recognition Workshops*, pp. 1–8, 2008.

Charles Spearman. The proof and measurement of association between two things. *American Journal of Physics*, 15(1):72–101, 1904.

Masashi Sugiyama and Shinichi Nakajima. Pool-based active learning in approximate linear regression. *Machine Learning*, 75(3):249–274, 2009.

Wenhui Tan, Xin Gao, Yiyang Li, Guangqi Wen, Peng Cao, Jinzhu Yang, Weiping Li, and Osmar R Zaiane. Exploring attention mechanism for graph similarity learning. *Knowledge-Based System*, 276:110739, 2023.

Runzhong Wang, Tianqi Zhang, Tianshu Yu, Junchi Yan, and Xiaokang Yang. Combinatorial learning of graph edit distance via dynamic embedding. In *IEEE/CVF Conference on Computer Vision and Pattern Recognition*, pp. 5241–5250, 2021.

Xiaoli Wang, Xiaofeng Ding, Anthony KH Tung, Shanshan Ying, and Hai Jin. An efficient graph indexing method. In *IEEE International Conference on Data Engineering*, pp. 210–221, 2012.

Yuefei Wu, Bin Shi, Bo Dong, Qinghua Zheng, and Hua Wei. The evidence contraction issue in deep evidential regression: Discussion and solution. In *Proceedings of the AAAI Conference on Artificial Intelligence*, pp. 21726–21734, 2024.

Zonghan Wu, Shirui Pan, Fengwen Chen, Guodong Long, Chengqi Zhang, and Philip S Yu. A comprehensive survey on graph neural networks. *IEEE Transactions on Neural Networks and Learning Systems*, 32(1): 4–24, 2020.

Haoyan Xu, Runjian Chen, Yunsheng Bai, Jie Feng, Ziheng Duan, Ke Luo, Yizhou Sun, and Wei Wang. Hierarchical and fast graph similarity computation via graph coarsening and deep graph learning, 2020.

Haoyan Xu, Ziheng Duan, Yueyang Wang, Jie Feng, Runjian Chen, Qianru Zhang, and Zhongbin Xu. Graph partitioning and graph neural network based hierarchical graph matching for graph similarity computation. *Neurocomputing*, 439:348–362, 2021.

Zuobing Xu, Ram Akella, and Yi Zhang. Incorporating diversity and density in active learning for relevance feedback. In *European Conference on Information Retrieval*, pp. 246–257, 2007.

Xifeng Yan, Philip S Yu, and Jiawei Han. Substructure similarity search in graph databases. In *Proceedings of the International Conference on Management of Data*, pp. 766–777, 2005.

Pinar Yanardag and SVN Vishwanathan. Deep graph kernels. In *Proceedings of the ACM SIGKDD Conference on Knowledge Discovery and Data Mining*, pp. 1365–1374, 2015.

Haoran Yang, Junli Wang, Rui Duan, Changwei Wang, and Chungang Yan. Disentangled active learning on graphs. *Neural Networks*, 185:107130, 2025a.

Wenjie Yang, Shengzhong Zhang, Jiaxing Guo, and Zengfeng Huang. Contra^2: A one-step active learning method for imbalanced graphs. *Artificial Intelligence*, 349:104439, 2025b.

Yi Yang, Zhigang Ma, Feiping Nie, Xiaojun Chang, and Alexander G Hauptmann. Multi-class active learning by uncertainty sampling with diversity maximization. *International Journal of Computer Vision*, 113(2): 113–127, 2015.

Kai Ye, Tiejin Chen, Hua Wei, and Liang Zhan. Uncertainty regularized evidential regression. In *Proceedings of the AAAI Conference on Artificial Intelligence*, pp. 16460–16468, 2024.

Donggeun Yoo and In So Kweon. Learning loss for active learning. In *IEEE/CVF Conference on Computer Vision and Pattern Recognition*, pp. 93–102, 2019.

Wentao Zhang, Yu Shen, Yang Li, Lei Chen, Zhi Yang, and Bin Cui. ALG: Fast and accurate active learning framework for graph convolutional networks. In *Proceedings of the International Conference on Management of Data*, pp. 2366–2374, 2021a.

Wentao Zhang, Yexin Wang, Zhenbang You, Meng Cao, Ping Huang, Jiulong Shan, Zhi Yang, and Bin Cui. RIM: Reliable influence-based active learning on graphs. In *Advances in Neural Information Processing Systems*, pp. 27978–27990, 2021b.

Wentao Zhang, Zhi Yang, Yexin Wang, Yu Shen, Yang Li, Liang Wang, and Bin Cui. Grain: Improving data efficiency of graph neural networks via diversified in fluence maximization. *Proceedings of the VLDB Endowment*, 14(11):2473–2482, 2021c.

Wentao Zhang, Yexin Wang, Zhenbang You, Meng Cao, Ping Huang, Jiulong Shan, Zhi Yang, and CUI Bin. Information gain propagation: A new way to graph active learning with soft labels. In *International Conference on Learning Representations*, 2022.

Zhen Zhang, Jiajun Bu, Martin Ester, Zhao Li, Chengwei Yao, Zhi Yu, and Can Wang. H^2MN: Graph similarity learning with hierarchical hypergraph matching networks. In *Proceedings of the ACM SIGKDD Conference on Knowledge Discovery and Data Mining*, pp. 2274–2284, 2021d.

Haoran Zheng, Jieming Shi, and Renchi Yang. GraSP: Simple yet effective graph similarity predictions. In *Proceedings of the AAAI Conference on Artificial Intelligence*, pp. 22884–22892, 2025.

Cuifang Zou, Guangquan Lu, Wenzhen Zhang, Xuxia Zeng, Shilong Lin, Longqing Du, and Shichao Zhang. Enhanced graph similarity learning via adaptive multi-scale feature fusion. In *Proceedings of the International Joint Conference on Artificial Intelligence*, pp. 7309–7317, 2025.

A Detailed Theoretical Derivation

We provide the detailed mathematical derivations for the uncertainty decomposition and the marginal likelihood objective used in our evidential framework. Let the predicted evidential parameters be $\mathbf{o} = \{\gamma, \nu, \alpha, \beta\}$. The Normal-Inverse-Gamma (NIG) prior over the unknown mean μ and variance σ^2 is defined as:

$$p(\mu, \sigma^2 \mid \mathbf{o}) = \mathcal{N}\left(\mu \mid \gamma, \frac{\sigma^2}{\nu}\right) \Gamma^{-1}(\sigma^2 \mid \alpha, \beta). \tag{11}$$

A.1 Derivation of Epistemic Uncertainty

The epistemic uncertainty $\mathcal{U}_{\text{epi}}$ captures the model's lack of knowledge about the true mean μ, which is quantified by the variance of μ. We derive this rigorously using the *Law of Total Variance*:

$$\mathcal{U}_{\text{epi}} = \text{Var}[\mu] = \mathbb{E}_{\sigma^2}[\text{Var}[\mu \mid \sigma^2]] + \text{Var}_{\sigma^2}[\mathbb{E}[\mu \mid \sigma^2]]. \tag{12}$$

From the conditional Gaussian distribution $(\mu \mid \sigma^2) \sim \mathcal{N}(\gamma, \sigma^2/\nu)$, we can determine the inner terms:

1. $\mathbb{E}[\mu \mid \sigma^2] = \gamma$. Since γ is a deterministic parameter output by the neural network and is constant with respect to σ^2, its variance is zero: $\text{Var}_{\sigma^2}[\gamma] = 0$.

2. $\text{Var}[\mu \mid \sigma^2] = \frac{\sigma^2}{\nu}$.

Substituting these into the total variance equation, the second term vanishes, yielding:

$$\text{Var}[\mu] = \mathbb{E}_{\sigma^2}\left[\frac{\sigma^2}{\nu}\right] = \frac{1}{\nu}\mathbb{E}_{\sigma^2}[\sigma^2]. \tag{13}$$

To compute $\mathbb{E}_{\sigma^2}[\sigma^2]$, we use the probability density function of the Inverse-Gamma distribution $\Gamma^{-1}(\alpha, \beta)$:

$$\mathbb{E}_{\sigma^2}[\sigma^2] = \int_0^\infty \sigma^2 \frac{\beta^\alpha}{\Gamma(\alpha)} (\sigma^2)^{-(\alpha+1)} \exp\left(-\frac{\beta}{\sigma^2}\right) d\sigma^2 = \frac{\beta^\alpha}{\Gamma(\alpha)} \int_0^\infty (\sigma^2)^{-\alpha} \exp\left(-\frac{\beta}{\sigma^2}\right) d\sigma^2. \tag{14}$$

Recognizing the integral part as the unnormalized form of an Inverse-Gamma distribution with parameters $(\alpha - 1, \beta)$, it evaluates to $\frac{\Gamma(\alpha-1)}{\beta^{\alpha-1}}$. Thus, for $\alpha > 1$:

$$\mathbb{E}_{\sigma^2}[\sigma^2] = \frac{\beta^\alpha}{\Gamma(\alpha)} \frac{\Gamma(\alpha-1)}{\beta^{\alpha-1}} = \frac{\beta}{\alpha - 1}. \tag{15}$$

Substituting this back, the epistemic uncertainty is analytically derived as:

$$\mathcal{U}_{\text{epi}} = \frac{\beta}{\nu(\alpha - 1)}. \tag{16}$$

A.2 Derivation of the Marginal Likelihood and Learning Objective

To formulate the learning objective, we compute the marginal likelihood $p(y \mid \mathbf{o})$ by integrating out the latent parameters μ and σ^2:

$$p(y \mid \mathbf{o}) = \int_0^\infty \int_{-\infty}^\infty p(y \mid \mu, \sigma^2) p(\mu, \sigma^2 \mid \mathbf{o}) \, d\mu \, d\sigma^2. \tag{17}$$

Step 1: Marginalizing out μ. Since the likelihood is $(y \mid \mu, \sigma^2) \sim \mathcal{N}(\mu, \sigma^2)$ and the prior is $(\mu \mid \sigma^2) \sim \mathcal{N}(\gamma, \sigma^2/\nu)$, the convolution of these two Gaussian distributions results in another Gaussian distribution for y conditioned only on σ^2:

$$p(y \mid \sigma^2, \mathbf{o}) = \int_{-\infty}^\infty \mathcal{N}(y \mid \mu, \sigma^2) \mathcal{N}\left(\mu \mid \gamma, \frac{\sigma^2}{\nu}\right) d\mu = \mathcal{N}\left(y \mid \gamma, \sigma^2 \left(1 + \frac{1}{\nu}\right)\right). \tag{18}$$

Step 2: Marginalizing out σ^2. We integrate the product of this new Gaussian and the Inverse-Gamma prior. Expanding the probability density functions, we get:

$$p(y \mid \mathbf{o}) = \int_0^\infty \frac{1}{\sqrt{2\pi\sigma^2(1 + 1/\nu)}} \exp\left(-\frac{(y-\gamma)^2}{2\sigma^2(1+1/\nu)}\right) \frac{\beta^\alpha}{\Gamma(\alpha)} (\sigma^2)^{-(\alpha+1)} \exp\left(-\frac{\beta}{\sigma^2}\right) d\sigma^2. \tag{19}$$

By grouping the terms involving σ^2, we can rewrite the integrand:

$$p(y \mid \mathbf{o}) = \frac{\beta^\alpha}{\Gamma(\alpha)\sqrt{2\pi(1+1/\nu)}} \int_0^\infty (\sigma^2)^{-(\alpha+\frac{1}{2}+1)} \exp\left(-\frac{1}{\sigma^2}\left(\beta + \frac{\nu(y-\gamma)^2}{2(1+\nu)}\right)\right) d\sigma^2. \tag{20}$$

The integral is exactly the unnormalized form of an Inverse-Gamma distribution with updated parameters $\tilde{\alpha} = \alpha + 1/2$ and $\tilde{\beta} = \beta + \frac{\nu(y-\gamma)^2}{2(1+\nu)}$. Evaluating this integral yields $\Gamma(\tilde{\alpha})/\tilde{\beta}^{\tilde{\alpha}}$. Therefore:

$$p(y \mid \mathbf{o}) = \frac{\Gamma(\alpha + 1/2)}{\Gamma(\alpha)\sqrt{2\pi(1+1/\nu)}} \frac{\beta^\alpha}{\left(\beta + \frac{\nu(y-\gamma)^2}{2(1+\nu)}\right)^{\alpha+1/2}}. \tag{21}$$

Connection to the Learning Objective. By factoring out β in the denominator, the expression matches the standard probability density function of a Student-t distribution $\mathrm{St}(y; \tilde{\mu}, \tilde{\sigma}^2, \tilde{v})$:

$$p(y \mid \mathbf{o}) = \mathrm{St}\left(y; \gamma, \frac{\beta(1+\nu)}{\nu\alpha}, 2\alpha\right), \tag{22}$$

where the location parameter is γ, the scale parameter is $\frac{\beta(1+\nu)}{\nu\alpha}$, and the degrees of freedom is 2α.

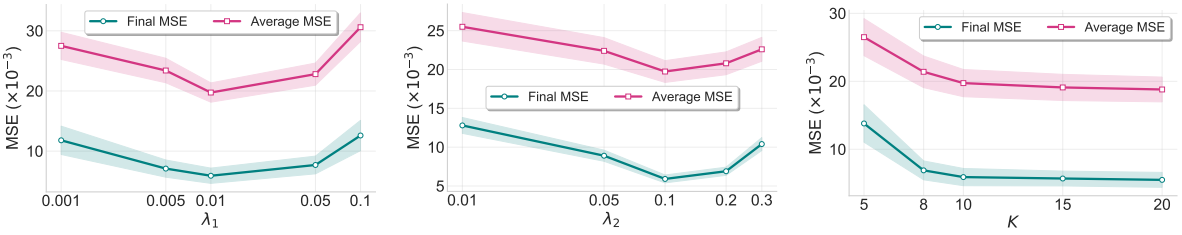

(a) Evidential regularizer λ_1 (b) MSE regularizer λ_2 (c) Reference subset size K

Figure 8: **Sensitivity analysis of EVGS** using SimGNN on the AIDS dataset.

B Detailed Experimental Results

B.1 Hyperparameter Sensitivity

To investigate the stability of EVGS, we conduct a sensitivity analysis on three key hyperparameters: the evidential regularizer coefficient λ_1, the MSE regularizer coefficient λ_2, and the reference subset size K. We report both the *Final MSE* (at the last active learning round) and the *Average MSE* (across all rounds) on the AIDS dataset using the SimGNN backbone. The results are illustrated in Figure 8.

Impact of Evidential Regularization Coefficient λ_1. Figure 8(a) displays the performance variation concerning the evidential regularizer λ_1. We observe a convex pattern: small values ($\lambda_1 < 0.005$) lead to under-regularization, where the model fails to penalize misleading evidence, while excessive regularization ($\lambda_1 > 0.05$) forces the distribution towards a uniform prior, hindering representation learning. The performance is robust within $[0.005, 0.05]$, peaking at $\lambda_1 = 0.01$.

Impact of MSE Regularizer Coefficient λ_2. Figure 8(b) examines the sensitivity to λ_2, which serves as the critical gradient anchor coefficient. The observed convex trend empirically validates our theoretical analysis regarding the *Low-Evidence Trap*. For small values λ_2 (e.g., < 0.05), the model lacks sufficient gradient injection to counteract the vanishing gradient pathology inherent to evidential regression. As detailed in our theoretical derivation, without this anchor, the optimization tends to collapse into a "uniform ignorance" state ($\nu \to 0^+$) where NLL gradients vanish. This results in a flattened uncertainty landscape, effectively degrading the AL strategy to random sampling. Conversely, when λ_2 is excessively large (e.g., > 0.2), the deterministic MSE loss overpowers the probabilistic NLL objective. While this enforces regression consistency, it suppresses the fine-grained learning of evidential parameters, rendering the derived epistemic uncertainty uncalibrated for sample ranking. The performance optimality at $\lambda_2 = 0.1$ confirms that this setting provides the necessary gradient flow to prevent evidence collapse while preserving the dominance of the evidential objective for uncertainty quantification.

Impact of Reference Subset Size K. Figure 8(c) investigates the size of the reference subset K used for graph-centric selection. While a larger K theoretically provides a more robust estimation of uncertainty variance, it incurs higher computational overhead. We observe that the performance gain saturates around $K = 10$. Consequently, we fix $K = 10$ for all experiments to achieve an optimal trade-off between estimation reliability and computational efficiency.

B.2 Comparison with Baselines

Performance comparisons on the AIDS and LINUX datasets are presented in Figure 9 and Figure 10, respectively. These results corroborate the trends reported in the main paper, demonstrating the generalizability of our EVGS across diverse graph domains.

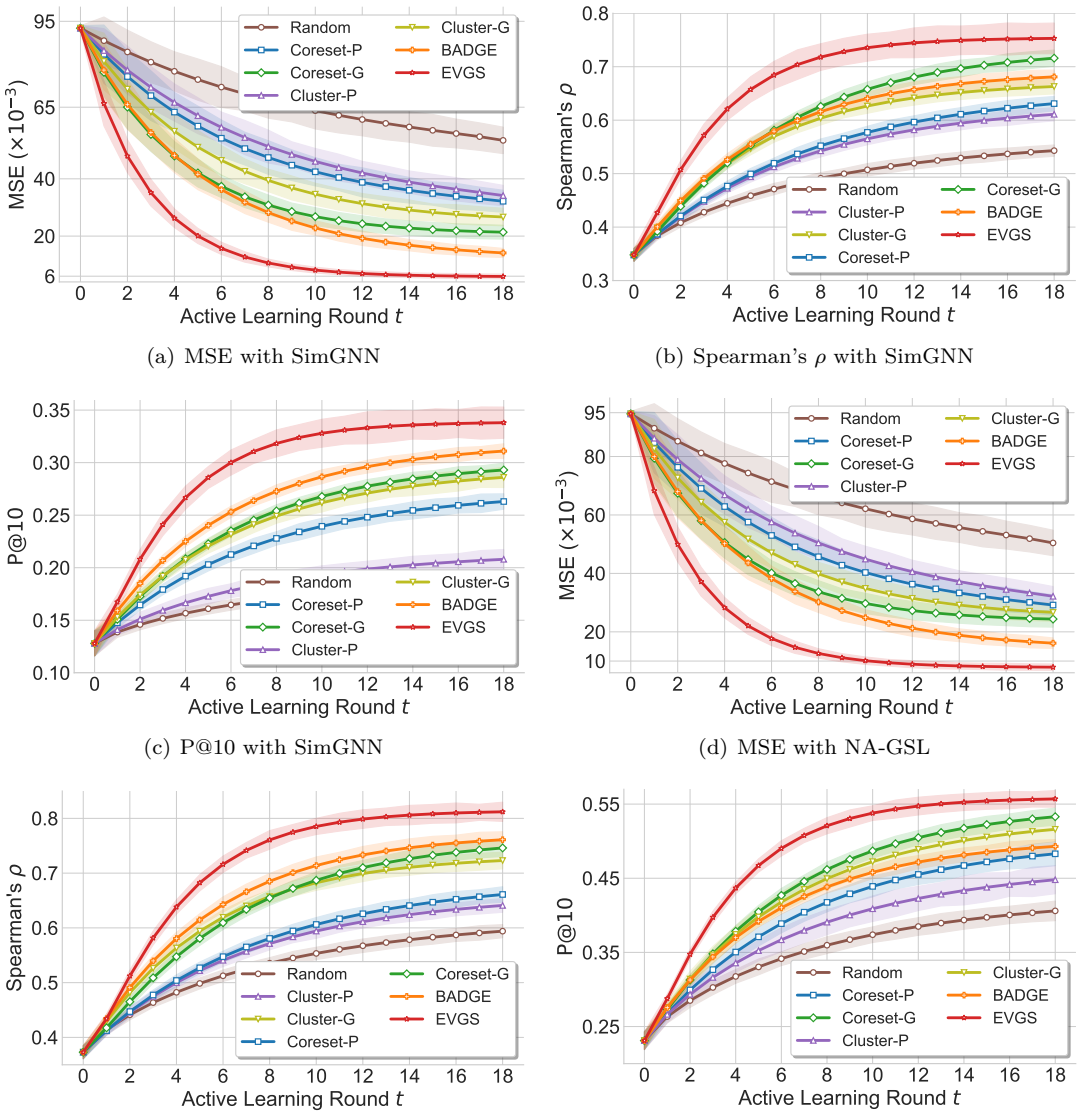

(a) MSE with SimGNN

(b) Spearman's ρ with SimGNN

(c) P@10 with SimGNN

(d) MSE with NA-GSL

(e) Spearman's ρ with NA-GSL

(f) P@10 with NA-GSL

Figure 9: **Performance comparison with baselines** on the AIDS dataset.

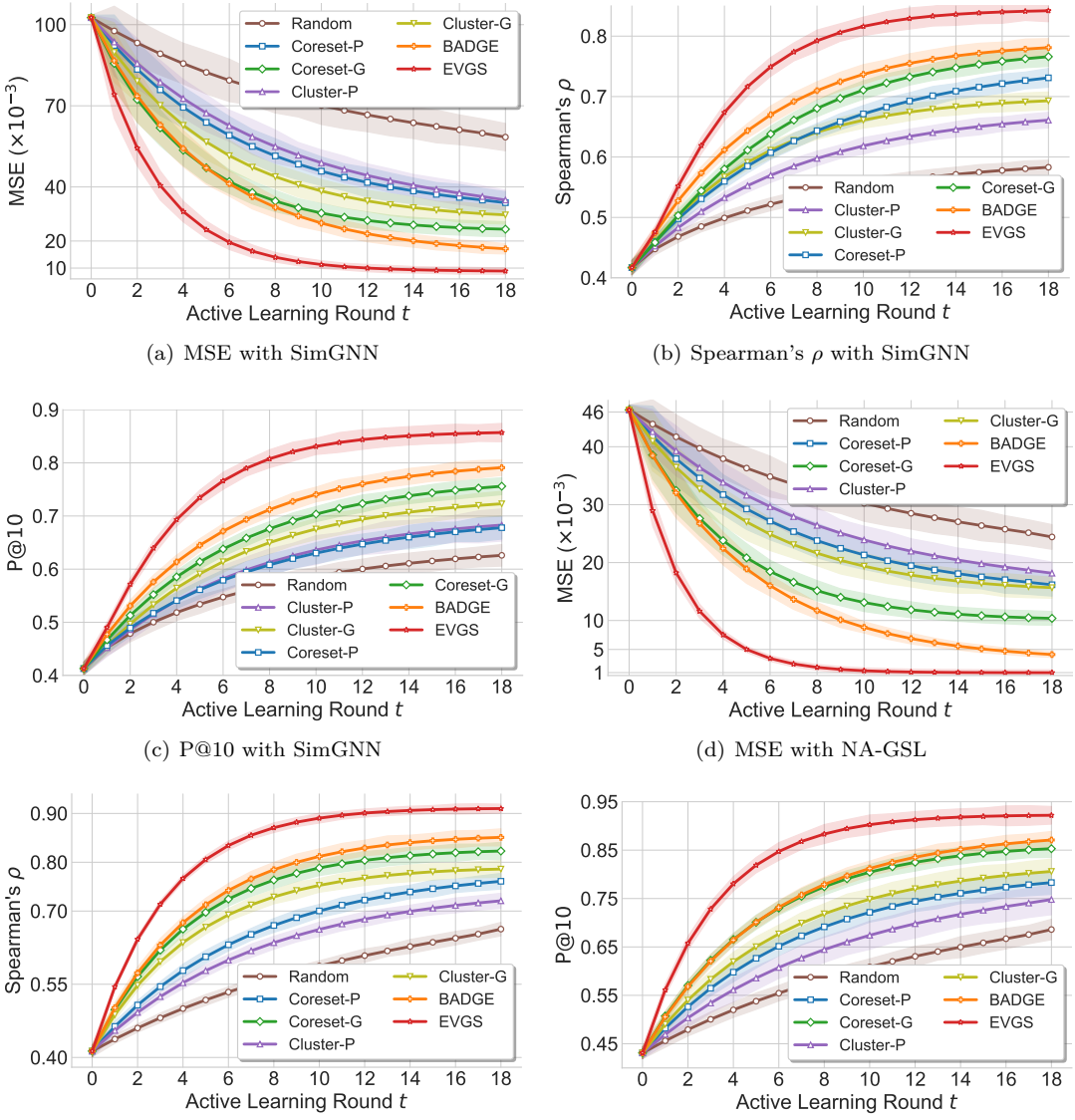

(a) MSE with SimGNN

(b) Spearman's ρ with SimGNN

(c) P@10 with SimGNN

(d) MSE with NA-GSL

(e) Spearman's ρ with NA-GSL

(f) P@10 with NA-GSL

Figure 10: **Performance comparison with baselines** on the LINUX dataset.